Eur. Phys. J. A **13**, 227–232 (2002)

THE EUROPEAN PHYSICAL JOURNAL A

Asymptotic normalization coefficients and astrophysical direct capture rates

C.A. Gagliardi[1], A. Azhari[1], V. Burjan[2], F. Carstoiu[3], V. Kroha[2], A.M. Mukhamedzhanov[1], A. Sattarov[1], X. Tang[1], L. Trache[1], and R.E. Tribble[1]

[1] Cyclotron Institute, Texas A&M University, College Station, TX 77843, USA
[2] Institute for Nuclear Physics, Czech Academy of Sciences, Prague-Řež, Czech Republic
[3] Institute for Atomic Physics, Bucharest, Romania

Received: 1 May 2001

Abstract. Peripheral transfer reactions can be used to determine asymptotic normalization coefficients (ANCs). These coefficients, which specify the normalization of the tail of the nuclear overlap function, determine S-factors for direct capture reactions at astrophysical energies. A variety of proton transfer reactions involving both stable and radioactive beams have been used to measure ANCs. Tests have demonstrated that ANCs determined from proton transfer reactions can be used to calculate astrophysical direct capture rates to within 9%. The ^{10}B(^{7}Be, ^{8}B)^{9}Be and ^{14}N(^{7}Be, ^{8}B)^{13}C reactions have been used to measure the ANC appropriate for determining the ^{7}Be$(p,\gamma)^{8}$B rate, and the ^{14}N(^{11}C, ^{12}N)^{13}C reaction has been used to measure the ANC required to calculate the ^{11}C$(p,\gamma)^{12}$N rate.

PACS. 26.20.+f Hydrostatic stellar nucleosynthesis – 25.60.Je Transfer reactions – 21.10.Jx Spectroscopic factors

1 Introduction

Stellar evolution involves sequences of direct and resonant capture reactions, together with beta-decays, whose rates must be known to make reliable predictions. Direct capture reactions of astrophysical interest usually involve systems where the binding energy of the captured proton is low. Hence at stellar energies, the capture proceeds through the tail of the nuclear overlap function. The shape of the overlap function in this tail region is completely determined by the Coulomb interaction, so the amplitude of the overlap function alone dictates the rate of the capture reaction. The ^{7}Be$(p,\gamma)^{8}$B reaction, which plays a central role in the solar neutrino problem, is an excellent example of such a direct capture process [1].

The asymptotic normalization coefficient (ANC) C for $A+p \leftrightarrow B$ specifies the amplitude of the tail of the overlap function of the bound state B in the two-body channel $(A\,p)$. We have pointed out [2,3] that astrophysical S-factors for peripheral direct radiative capture reactions can be determined through measurements of ANCs using traditional nuclear reactions such as peripheral nucleon transfer. Direct capture S-factors derived with this technique are most reliable at the lowest incident energies in the capture reaction, precisely where capture cross-sections are the smallest and most difficult to measure directly. It is extremely important to test the reliability of the ANC technique in order to know the precision with which it can be applied. Below we give a brief description of this technique and discuss three tests that have been performed. We shall then describe our ^{10}B(^{7}Be,^{8}B)^{9}Be, ^{14}N(^{7}Be,^{8}B)^{13}C, and ^{14}N(^{11}C,^{12}N)^{13}C radioactive beam studies and their use to determine the astrophysical S-factors for ^{7}Be$(p,\gamma)^{8}$B and ^{11}C$(p,\gamma)^{12}$N.

2 ANCs from proton transfer reactions

Traditionally, spectroscopic factors have been obtained from DWBA analysis of proton transfer reactions. However, it is well known that these spectroscopic factors have significant systematic uncertainties associated with the choice of proton single-particle orbitals in the initial and final nuclei. For peripheral transfer reactions, the ANC is better determined and is the more natural quantity to extract. Consider the proton transfer reaction $a+A \to c+B$, where $a = c+p$, $A+p = B$. As was previously shown [3], we can write the DWBA cross-section in the form

$$\frac{\mathrm{d}\sigma}{\mathrm{d}\Omega} = \sum_{j_B j_a} (C^{B}_{Apl_B j_B})^2 (C^{a}_{cpl_a j_a})^2 \frac{\sigma^{\mathrm{DW}}_{l_B j_B l_a j_a}}{b^2_{Apl_B j_B} b^2_{cpl_a j_a}}, \qquad (1)$$

where $\sigma^{\mathrm{DW}}_{l_B j_B l_a j_a}$ is the reduced DWBA cross-section and j_i, l_i are the total and orbital angular momenta of the transferred proton in nucleus i. The factors $b_{cpl_a j_a}$ and

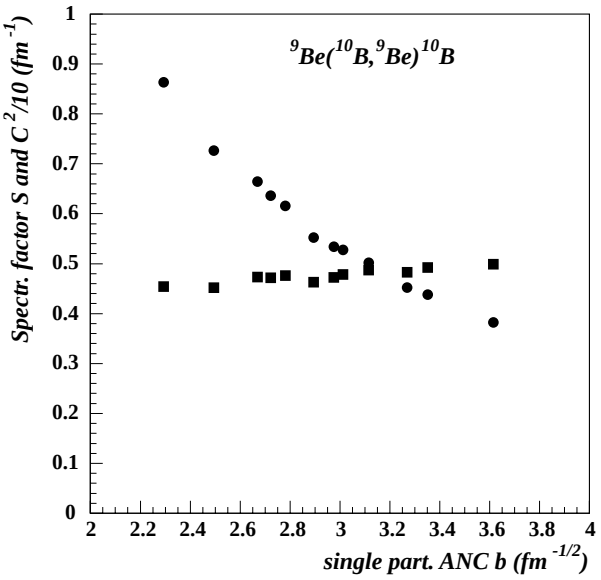

Fig. 1. The dependence of the spectroscopic factor S (circles) and the ANC C^2 (squares) for $^{10}\mathrm{B} \leftrightarrow {}^9\mathrm{Be} + p$ on the single-particle ANC b used in the DWBA analysis of the $^9\mathrm{Be}(^{10}\mathrm{B}, {}^9\mathrm{Be})^{10}\mathrm{B}$ reaction [3].

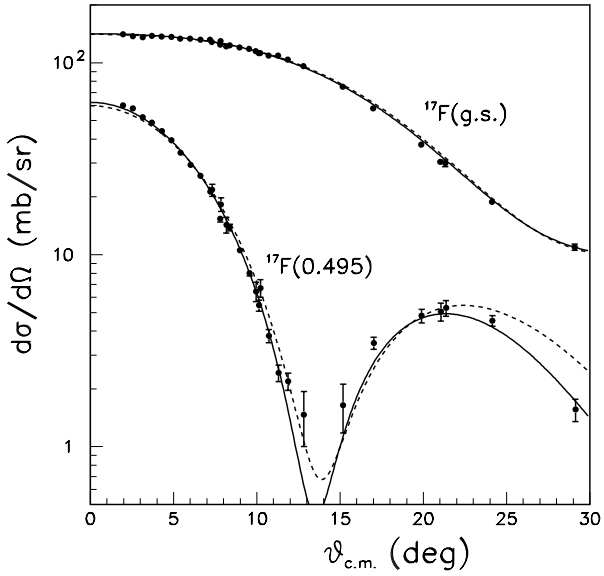

Fig. 2. DWBA fits to the $^{16}\mathrm{O}(^3\mathrm{He}, d)^{17}\mathrm{F}$ reaction, populating the ^{17}F ground and first-excited states. The absolute magnitudes of the cross-sections determine the correponding ANCs [6].

$b_{Apl_Bj_B}$ are the ANCs of the bound-state proton wave functions in nuclei a and B. If the reaction under consideration is peripheral, the ratio in eq. (1) is independent of $b_{Apl_Bj_B}$ and $b_{cpl_aj_a}$. Thus for surface reactions, the DWBA cross-section is best parametrized in terms of the product of the squares of the ANCs of the initial and final nuclei, $(C^B)^2(C^a)^2$, rather than spectroscopic factors. This is illustrated in fig. 1, which shows the strong sensitivity of the spectroscopic factor for $^{10}\mathrm{B} \leftrightarrow {}^9\mathrm{Be} + p$, and the independence of the corresponding ANC, on the assumed value of b when analyzing data for the $^9\mathrm{Be}(^{10}\mathrm{B}, {}^9\mathrm{Be})^{10}\mathrm{B}$ reaction. But it is also worth noting that, like the spectroscopic factor, the ANC inferred from a DWBA analysis of a peripheral proton transfer reaction is sensitive to the choice of optical potentials, so it is important that the potentials in the entrance and exit channels be well determined.

We have used this formulation to extract ANCs for $^{10}\mathrm{B} \leftrightarrow {}^9\mathrm{Be} + p$, $^{14}\mathrm{N} \leftrightarrow {}^{13}\mathrm{C} + p$, and $^{17}\mathrm{F} \leftrightarrow {}^{16}\mathrm{O} + p$ from the reactions $^9\mathrm{Be}(^{10}\mathrm{B},{}^9\mathrm{Be})^{10}\mathrm{B}$, $^{13}\mathrm{C}(^{14}\mathrm{N},{}^{13}\mathrm{C})^{14}\mathrm{N}$, $^{13}\mathrm{C}(^3\mathrm{He}, d)^{14}\mathrm{N}$, and $^{16}\mathrm{O}(^3\mathrm{He}, d)^{17}\mathrm{F}$. The first two reaction studies were carried out with beams from the K500 superconducting cyclotron at Texas A&M University. The $^{13}\mathrm{C}(^3\mathrm{He}, d)^{14}\mathrm{N}$ reaction was investigated at the U-120M isochronous cyclotron of the Nuclear Physics Institute of the Czech Academy of Sciences. The $^{16}\mathrm{O}(^3\mathrm{He}, d)^{17}\mathrm{F}$ reaction was studied at both laboratories. Figure 2 shows typical DWBA fits used to determine ANCs. Details of the experiments can be found in [3–6].

The two independent measurements of the $^{14}\mathrm{N} \leftrightarrow {}^{13}\mathrm{C} + p$ ANCs provide an important consistency check on our ability to extract ANCs from both light- and heavy-ion induced proton transfer reactions. We find the ANC for the dominant $p_{1/2}$ component of the ^{14}N ground state to be $C^2 = 18.6 \pm 1.2$ fm^{-1} from the $^{13}\mathrm{C}(^{14}\mathrm{N},{}^{13}\mathrm{C})^{14}\mathrm{N}$ reaction [4] and 17.8 ± 1.3 fm^{-1} from the $^{13}\mathrm{C}(^3\mathrm{He},d)^{14}\mathrm{N}$ reaction [5]. We adopted the weighted average of these two results below when analyzing the $^{14}\mathrm{N}(^7\mathrm{Be}, {}^8\mathrm{B})^{13}\mathrm{C}$ and $^{14}\mathrm{N}(^{11}\mathrm{C}, {}^{12}\mathrm{N})^{13}\mathrm{C}$ reactions. This would not have been possible with the spectroscopic factors determined from the DWBA fits to $^{13}\mathrm{C}(^{14}\mathrm{N}, {}^{13}\mathrm{C})^{14}\mathrm{N}$ and $^{13}\mathrm{C}(^3\mathrm{He}, d)^{14}\mathrm{N}$ because, like the case shown in fig. 1, the inferred spectroscopic factors for these reactions are very sensitive to the choice of single-particle bound-state orbitals in the DWBA calculations.

The ANCs for $^{10}\mathrm{B} \leftrightarrow {}^9\mathrm{Be} + p$ have been used in the analysis of the $^{10}\mathrm{B}(^7\mathrm{Be}, {}^8\mathrm{B})^9\mathrm{Be}$ reaction and to predict the direct capture contribution to the $^9\mathrm{Be}(p,\gamma)^{10}\mathrm{B}$ astrophysical S-factor. The ANCs for $^{17}\mathrm{F} \leftrightarrow {}^{16}\mathrm{O} + p$ have been used to predict the astrophysical S-factor for $^{16}\mathrm{O}(p,\gamma)^{17}\mathrm{F}$. The results are discussed below.

3 Testing the ANC technique

The ANCs found from the proton transfer reactions can be used to determine direct capture rates at astrophysical energies. The relation of the ANCs to the direct capture rate at low energies is straightforward to obtain. The cross-section for the direct capture reaction $A+p \rightarrow B+\gamma$ can be written as

$$\sigma = \lambda \mid \langle I^B_{Ap}(\mathbf{r}) \mid \hat{O}(\mathbf{r}) \mid \psi_i^{(+)}(\mathbf{r}) \rangle \mid^2, \qquad (2)$$

where λ contains kinematic factors, I^B_{Ap} is the overlap function for $B \rightarrow A+p$, $\hat{O}$ is the electromagnetic transition operator, and $\psi_i^{(+)}$ is the scattering wave in the incident channel. If the dominant contribution to the matrix element comes from outside the nuclear radius, the overlap

function may be replaced by

$$I^B_{Ap}(r) \approx C \frac{W_{-\eta,l+1/2}(2\kappa r)}{r}, \qquad (3)$$

where C defines the amplitude of the tail of the radial overlap function I^B_{Ap}, W is the Whittaker function, η is the Coulomb parameter for the bound state $B = A + p$, and κ is the bound-state wave number. The required C's are just the ANCs found above from transfer reactions. Thus, the direct capture cross-sections are directly proportional to the squares of these ANCs.

Using the ANCs mentioned above, the $^{16}\mathrm{O}(p,\gamma)^{17}\mathrm{F}$ S-factors for capture to the ground and first-excited states were calculated, with no additional normalization constants. The results [6] are shown in fig. 3, compared to the two previous measurements of $^{16}\mathrm{O}(p,\gamma)^{17}\mathrm{F}$ [7,8]. The theoretical uncertainty in the S-factors is less than 2% for energies below 1 MeV. The agreement between the measured S-factors and those calculated from our $^{17}\mathrm{F} \leftrightarrow {}^{16}\mathrm{O} + p$ ANCs is quite good. Overall, the results verify that the technique is valid for determining S-factors to accuracies of at least 9%.

The S-factor for $^{9}\mathrm{Be}(p,\gamma)^{10}\mathrm{B}$ has contributions from resonances and direct capture at stellar energies. Thus the connection between the ANC and the capture cross-section is more complicated [9]. Our measurement of the ANCs for $^{10}\mathrm{B} \leftrightarrow {}^{9}\mathrm{Be} + p$ fixes the nonresonant component. With this result, an R-matrix fit [9] was made to the existing data [10], using the known locations and widths of the resonances. Figure 3 shows that the fit does an excellent job of reproducing the data. Prior to our determination of the direct capture contribution, attempts to fit the data required substantial changes in the known resonance parameters.

Recently, the ANC technique has been tested in a neutron capture reaction for the first time. The ANC for $^{12}\mathrm{C} + n \leftrightarrow {}^{13}\mathrm{C}(1/2^+, 3.09\ \mathrm{MeV})$, measured in the $^{12}\mathrm{C}(d,p)^{13}\mathrm{C}$ reaction, has been found to predict the corresponding direct capture rate to better than 20% [11].

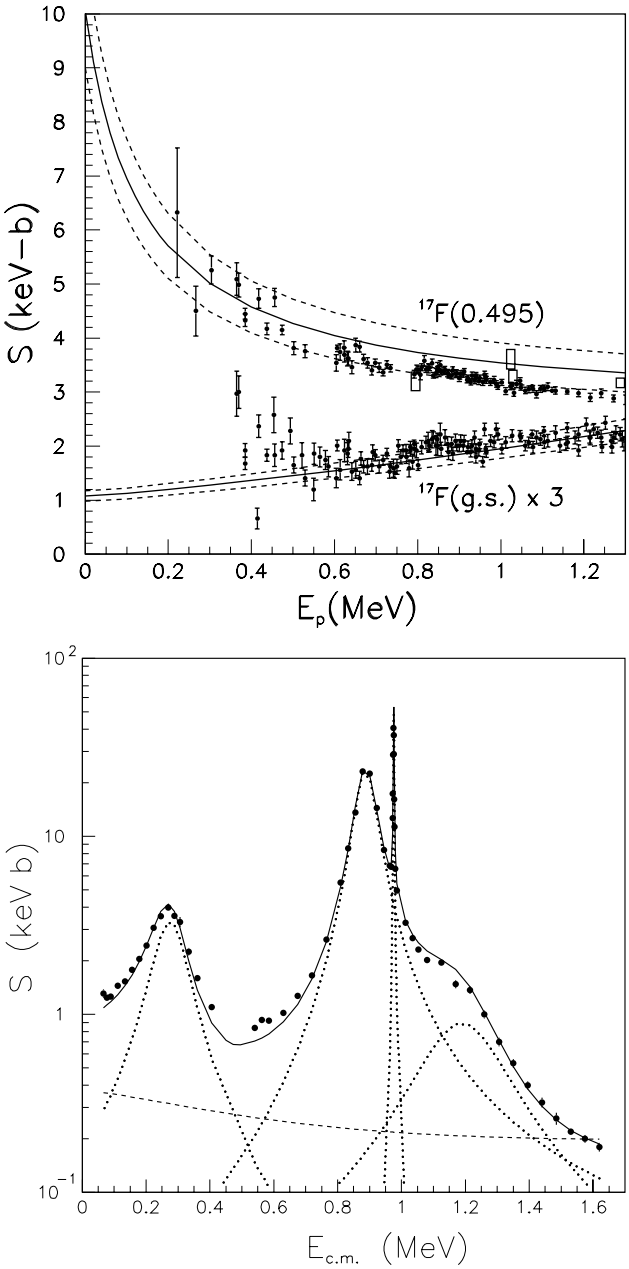

Fig. 3. A comparison of the experimental S-factors for $^{16}\mathrm{O}(p,\gamma)^{17}\mathrm{F}$ (upper panel) and $^{9}\mathrm{Be}(p,\gamma)^{10}\mathrm{B}$ (lower panel) to those determined from the ANCs found in $^{16}\mathrm{O}(^3\mathrm{He},d)^{17}\mathrm{F}$ and $^{9}\mathrm{Be}(^{10}\mathrm{B},{}^{9}\mathrm{Be})^{10}\mathrm{B}$. The solid curves are the results described in the text. In the upper panel, the dashed curves show 1σ error bands. In the lower panel, the dashed curve shows the direct capture contribution and the dotted curves show the resonances.

4 Optical potentials for radioactive beams

As noted above, it is necessary to know the corresponding optical potentials to extract ANCs from proton transfer reactions. Typically radioactive beam intensities are too small to measure the elastic scattering over the broad angular range required to obtain unambiguous optical model parameters. Consequently, we have carried out a series of elastic scattering measurements of $1p$ shell nuclei with stable beam and target combinations that are close to those in our radioactive beam measurements. We used the double-folding model prescription to determine the shape of the optical potentials, and then renormalized the real and imaginary parts of the potentials to fit the data [12]. Several different interactions were tried. The most stable results for loosely bound $1p$ shell nuclei were found with the JLM effective interaction [13]. An important feature of the JLM interaction is that, unlike many other common effective interactions, it includes separate real and imaginary parts. The real potential was found to require a significant renormalization (0.366 ± 0.014) due to dynamic polarization effects for loosely bound nuclei that are not fully accounted for in the folding model. Consistent results were found for cases where one or both of the interacting nuclei were loosely bound. Larger renormalization constants for the real potential provided better fits

when both nuclei were tightly bound. No renormalization of the imaginary potential was required.

5 (^{7}Be, ^{8}B) reactions and ^{7}Be(p, γ)^{8}B

We have measured the (^{7}Be, ^{8}B) reaction on a 1.7 mg/cm^2 ^{10}B target [14] and a 1.5 mg/cm^2 Melamine target [15] in order to extract the ANC for ^{8}B $\leftrightarrow$ ^{7}Be + p. The radioactive ^{7}Be beam was produced at 12 MeV/u by filtering reaction products from the ^{1}H(^{7}Li,^{7}Be)n reaction in the recoil spectrometer MARS, starting with a primary ^{7}Li beam from the Texas A&M K500 cyclotron. Reaction products were measured by 5 $\times$ 5 cm^2 Si detector telescopes consisting of 100 μm ΔE strip detectors, with 16 position-sensitive strips, followed by 1000 μm E counters. An additional 1000 μm Si strip detector was used for ^{7}Be beam tuning. This detector, which was inserted at the target location, allowed us to optimize the beam shape and to normalize the ^{7}Be flux relative to a Faraday cup that measured the intensity of the primary ^{7}Li beam. The approximate ^{7}Be beam size was 6 mm $\times$ 3 mm (FWHM), the energy spread was $\approx$ 1.6 MeV, the full angular spread was $\Delta\theta \approx 28$ mrad and $\Delta\phi \approx 62$ mrad, and the purity was $\geq$ 99.5% ^{7}Be for the experiment with the ^{10}B target. The beam size and angular spread were improved for the experiment with the ^{14}N target to 4 mm $\times$ 3 mm and 21 mrad $\times$ 32 mrad. The beam detector was inserted periodically over the course of the experiment to check the stability of the secondary beam tune. The system was found to be quite stable, with maximum relative intensity changes of less than 5%.

Elastic scattering angular distributions are shown in fig. 4. For the ^{10}B target, the elastic scattering yield includes contributions from four target components —^{10}B, ^{11}B, C, and O— while the Melamine target includes ^{14}N, C, and H. A Monte Carlo simulation was used to generate the solid angle factor for each angular bin and the smoothing needed to account for the finite angular resolution. The absolute cross-section is then fixed by the target thickness, number of incident ^{7}Be, the yield in each bin, and the solid angle. The curves shown in fig. 4 were obtained from calculations using the double-folding model optical potentials for loosely bound 1p shell nuclei described in sect. 4. The cross-section predictions for the various target components were added together in the laboratory frame and then transformed to the center of mass assuming kinematics appropriate for the ^{10}B or ^{14}N targets. In both cases, the optical model calculations are compared to the data without additional normalization coefficients. The detector resolution is not sufficient to distinguish inelastic excitations from elastic scattering. This likely explains why the data exceed the calculations in the minima. The agreement between the measured absolute cross-sections and the optical model predictions is excellent.

The measured angular distributions for the (^{7}Be, ^{8}B) reactions populating the ground states of ^{9}Be and ^{13}C are shown in fig. 5, where they are compared to DWBA predictions that use the same procedure as for the elastic scattering. Two ^{8}B orbitals, $1p_{1/2}$ and $1p_{3/2}$, contribute to the transfer reactions, but the $1p_{3/2}$ dominates in both cases. Only the $1p_{3/2}$ orbital in ^{10}B contributes. Both $1p_{1/2}$ and $1p_{3/2}$ contribute for ^{14}N, with $1p_{1/2}$ dominating. The normalization factors between the data and the DWBA calculations determine the ANCs for ^{8}B $\leftrightarrow$ ^{7}Be + p, since the ANCs at the other vertices have been measured as described in sect. 2.

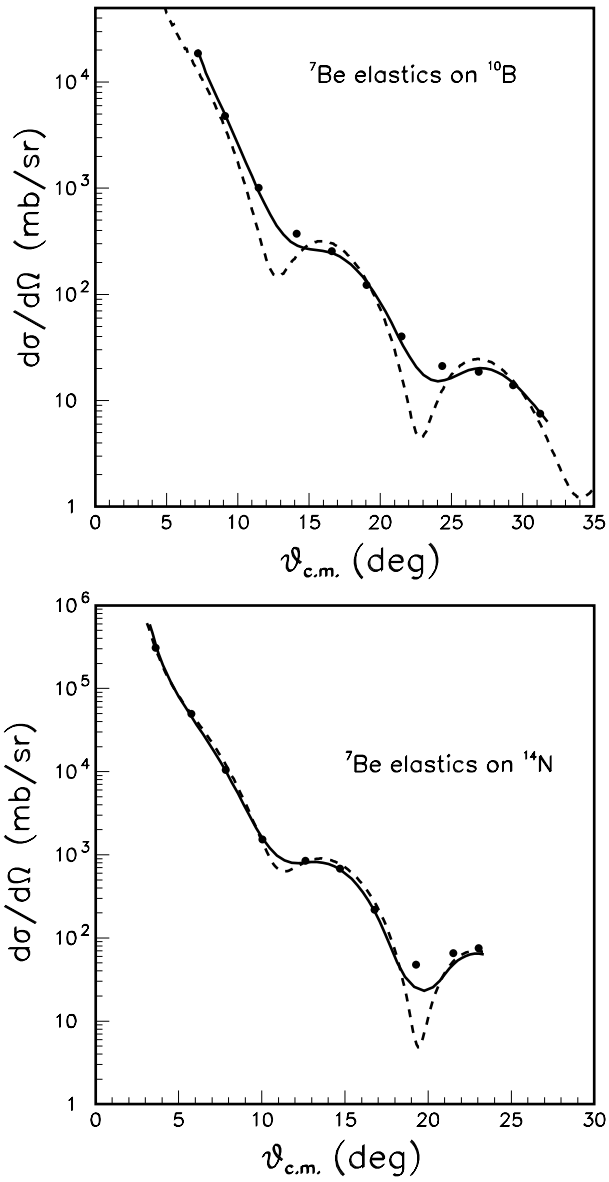

Fig. 4. Angular distributions for ^{7}Be elastic scattering from the ^{10}B and ^{14}N targets. The dashed curves are optical model predictions and the solid curves are smoothed over the angular acceptance of each bin.

To investigate the influence of multi-step processes on the extracted ANC, we have performed coupled-channels Born approximation calculations of the ^{10}B(^{7}Be, ^{8}B)^{9}Be reaction [16]. This reaction was chosen because the large

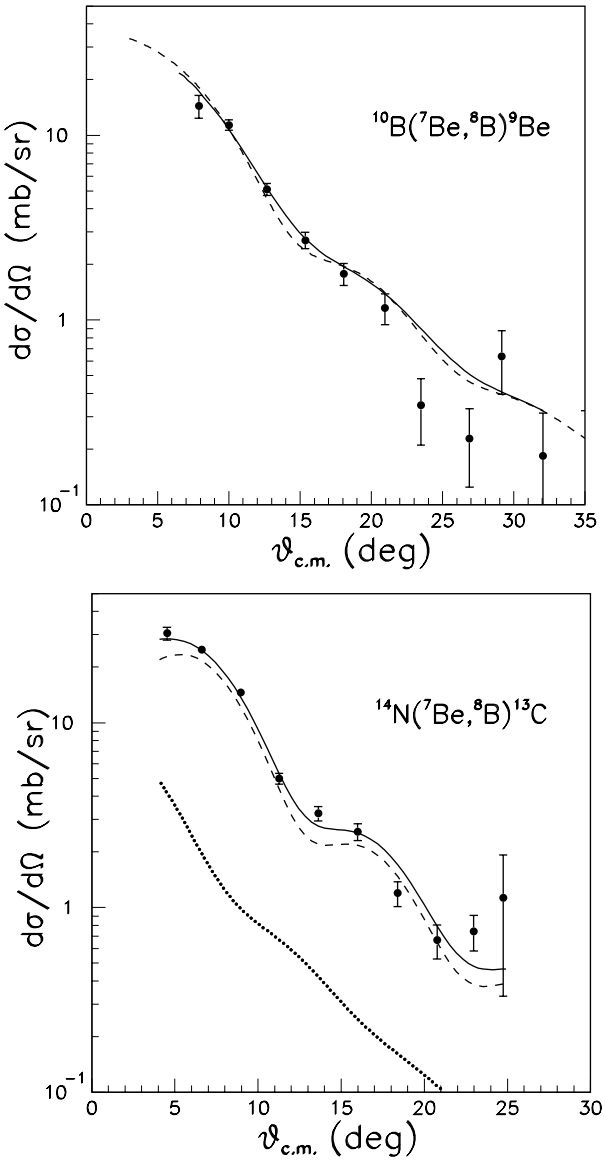

Fig. 5. Angular distributions for ^{8}B populating the ground state of ^{9}Be from the ^{10}B target and ^{13}C from the Melamine target. In the upper figure, the dashed curve shows the result of a DWBA calculation for the dominant component that contributes to the cross-section. Two components are shown in the lower figure. In both cases, the solid curve is smoothed over the angular acceptance of each bin.

static deformation of ^{10}B may enhance the importance of multi-step effects. Inelastic excitations in both ^{9}Be and ^{10}B were included, as well as proton transfers between the various excited states. We found that fitting the measured angular distribution to the result of the coupled-channels calculation changed the extracted ANC for $^8\mathrm{B} \leftrightarrow {}^7\mathrm{Be} + p$ by only 3%.

The results of the two (^{7}Be, ^{8}B) reaction studies have correlated uncertainties due to the common choice of optical model parameters. Combining the results, accounting for this correlation, we conclude that the $^7\mathrm{Be}(p,\gamma)^8\mathrm{B}$ capture rate is 17.3 ± 1.8 eV b, in good agreement with the recommended value [1] of 19^{+4}_{-2} eV b.

6 ^{14}N(^{11}C, ^{12}N)^{13}C and ^{11}C(p, γ)^{12}N

First-generation stars were composed entirely of nuclei produced in the Big Bang. Thus, such stars could only undergo nucleosynthesis via the *pp* chains or the triple-alpha process until heavier nuclei were produced to initiate the CNO cycle. Fuller *et al.* [17] have shown that, for super-massive first generation stars, the standard *pp* chains that operate within our Sun generate too little energy and the triple-alpha reaction turns on too late to cause an explosion. Rather, such stars simply collapse to black holes. Thus, they would play no role in later galactic chemical evolution. More recently, Wiescher *et al.* [18] have noted that hot *pp* chains that were neglected in the earlier work may provide a path for low-metallicity, supermassive stars to produce CNO nuclei at a lower temperature than required by the triple-alpha reaction. These CNO nuclei might then serve as seeds for further energy generation, stablizing the star against collapse long enough to permit an explosion to occur.

The $^{11}\mathrm{C}(p,\gamma)^{12}\mathrm{N}$ reaction is an important branch point in the hot *pp* chains. In massive objects, ^{11}C is produced efficiently via the $^7\mathrm{Be}(\alpha,\gamma)^{11}\mathrm{C}$ reaction at temperatures above 0.2 GK. Its fate then depends on the competition between ^{11}C proton capture and beta-decay, and photodisintegration of ^{12}N. If the density is sufficiently high that proton capture dominates, ^{11}C will provide a path to produce CNO nuclei. At lower densities, the path will be blocked by the $^{11}\mathrm{B}(p,3\alpha)$ reaction following ^{11}C beta-decay. There have been two previous investigations of the $^{11}\mathrm{C}(p,\gamma)^{12}\mathrm{N}$ reaction, both using Coulomb breakup of ^{12}N [19,20], which have obtained conflicting results.

We have measured the $^{14}\mathrm{N}(^{11}\mathrm{C},^{12}\mathrm{N})^{13}\mathrm{C}$ reaction to determine the ANC for $^{11}\mathrm{C} + p \leftrightarrow {}^{12}\mathrm{N}$ and, in turn, the direct capture rate for $^{11}\mathrm{C}(p,\gamma)^{12}\mathrm{N}$ at astrophysical energies. The experiment used a ^{11}C radioactive beam, with an intensity of $\sim 4.2 \times 10^5$ particles/s at an energy of 10 MeV/u, incident on a 1.5 mg/cm^2 Melamine target. The radioactive beam was produced in the reaction $^1\mathrm{H}(^{11}\mathrm{B},{}^{11}\mathrm{C})n$ and filtered by MARS, using procedures similar to those in the (^{7}Be, ^{8}B) measurements described in the previous section.

Both ^{11}C elastic scattering off the Melamine target and (^{11}C, ^{12}N) proton transfer reactions were observed simultaneously. Figure 6 shows the preliminary results for the measured elastic scattering distribution, together with two theoretical predictions, each of which has already been smoothed to account for finite angular acceptance. As above, the absolute cross-sections predicted by the optical potentials are compared to the data without additional normalization coefficients. The dot-dashed curve uses the double-folding optical potential for loosely bound 1*p* shell nuclei described in sect. 4 and provides a poor description of the data beyond 20°. However, one should note

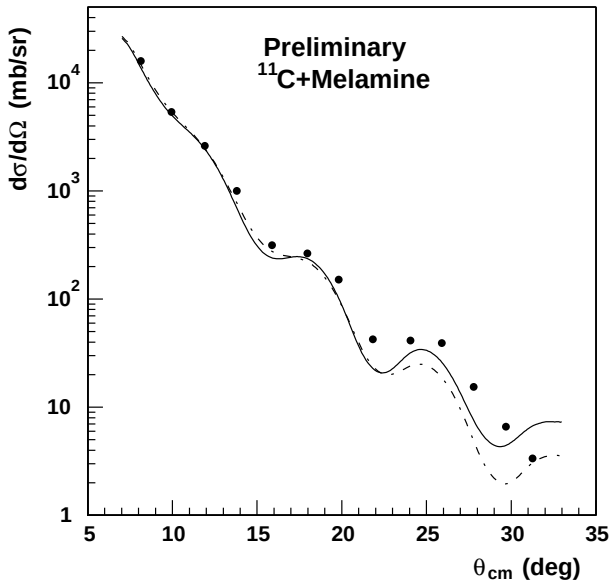

Fig. 6. Preliminary angular distribution for ^{11}C elastic scattering from the Melamine target. The curves are two optical model predictions, as described in the text.

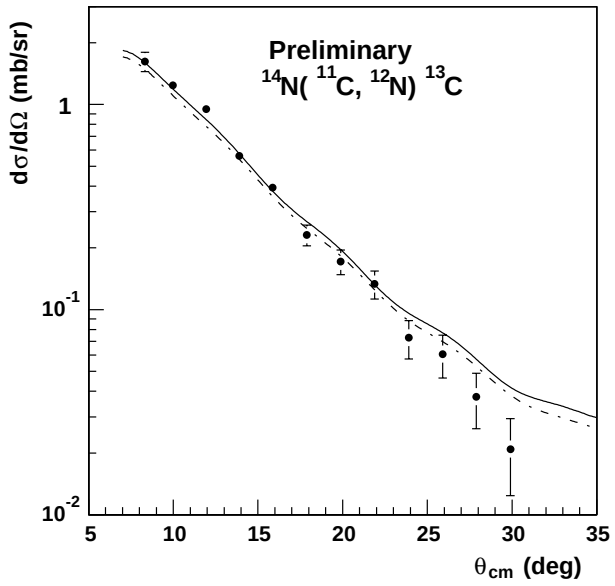

Fig. 7. Preliminary angular distribution for the ^{14}N(^{11}C, ^{12}N)^{13}C reaction. The curves represent DWBA predictions of the angular distribution obtained using the same optical potentials as in fig. 6. The solid curve has been normalized to the data. The dot-dashed curve uses the same normalization constant as the solid curve.

that ^{11}C is not loosely bound, so the renormalization of the real potential should not be as great. The solid curve uses the same normalization factors for the double-folding optical potential that provided the best fit to ^{13}C + ^{14}N elastic scattering [12], and provides a better description of the data.

Figure 7 shows our preliminary angular distribution for the ^{14}N(^{11}C,^{12}N)^{13}C reaction. The solid curve is a DWBA prediction of the proton transfer reaction that uses the same optical potential for ^{11}C + ^{14}N as in the solid curve in fig. 6, and uses the optical potential described in sect. 4 for ^{12}N + ^{13}C. The normalization of this DWBA prediction to the data determines the ANC for $^{12}\mathrm{N} \leftrightarrow {}^{11}\mathrm{C} + p$. The dot-dashed curve is a DWBA prediction that uses the optical potential described in sect. 4 in both the entrance and exit channels and the same normalization as the solid curve. It demonstrates that the sensitivity of the elastic scattering distribution to the choice of double-folding potential renormalization factors illustrated in fig. 6 leads to an uncertainty in the inferred ANC for $^{12}\mathrm{N} \leftrightarrow {}^{11}\mathrm{C} + p$ of only 4%. Our preliminary results indicate that the direct capture contribution to the $^{11}\mathrm{C}(p,\gamma)^{12}\mathrm{N}$ S-factor is significantly larger than assumed in [18] or found in [19]. This will reduce the stellar density required for the proton capture reaction, leading to the production of CNO nuclei, to compete successfully with ^{11}C beta-decay and ^{12}N photodisintegration.

This work was supported in part by the U. S. Department of Energy under Grant No. DE-FG03-93ER40773 and by the Robert A. Welch Foundation.

References

1. E.G. Adelberger *et al.*, Rev. Mod. Phys. **70**, 1265 (1998).
2. H.M. Xu *et al.*, Phys. Rev. Lett. **73**, 2027 (1994).
3. A.M. Mukhamedzhanov *et al.*, Phys. Rev. C **56**, 1302 (1997).
4. L. Trache *et al.*, Phys. Rev. C **58**, 2715 (1998).
5. P. Bem *et al.*, Phys. Rev. C **62**, 024320 (2000).
6. C.A. Gagliardi *et al.*, Phys. Rev. C **59**, 1149 (1999).
7. R. Morlock *et al.*, Phys. Rev. Lett. **79**, 3837 (1997).
8. H.C. Chow, G.M. Griffith, T.H. Hall, Can. J. Phys. **53**, 1672 (1975).
9. A. Sattarov *et al.*, Phys. Rev. C **60**, 035801 (1999).
10. D. Zhanow *et al.*, Nucl. Phys. A **589**, 95 (1995).
11. N. Imai *et al.*, Nucl. Phys. A **688**, 281c (2001).
12. L. Trache *et al.*, Phys. Rev. C **61**, 024612 (2000).
13. J.P. Jeukenne, A. Lejeune, and C. Mahaux, Phys. Rev. C **16**, 80 (1977).
14. A. Azhari *et al.*, Phys. Rev. Lett. **82**, 3960 (1999).
15. A. Azhari *et al.*, Phys. Rev. C **60**, 035801 (1999).
16. A. Azhari *et al.*, Phys. Rev. C. **63**, 055803 (2001).
17. G.M. Fuller, S.E. Woosley, T.A. Weaver, Astrophys. J. **307**, 675 (1986).
18. M. Wiescher *et al.*, Astrophys. J. **343**, 352 (1989).
19. A. Lefebvre *et al.*, Nucl. Phys. A **592**, 69 (1995).
20. T. Motobayashi, *Proceedings of the 2nd Interanational Conference on Exotic Nuclei and Atomic Masses*, edited by B.M. Sherrill, D.J. Morrissey, C.N. Davids, AIP Conf. Proc. Vol. **455** (AIP, New York, 1998) p. 882.